Published in final edited form as:
Mol Microbiol. 2010 July 1; 77(1): 74–89. doi:10.1111/j.1365-2958.2010.07223.x.

A protein critical for cell constriction in the Gram-negative bacterium *Caulobacter crescentus* localizes at the division site through its peptidoglycan-binding LysM domains

Sebastian Poggio[1,§], **Constantin N. Takacs**[1,†], **Waldemar Vollmer**[2], and **Christine Jacobs-Wagner**[1,3,4,*]

[1] Department of Molecular, Cellular and Developmental Biology,Yale University, New Haven, CT 06511, USA.

[2] Institute for Cell and Molecular Biosciences, Newcastle University, Newcastle upon Tyne, UK.

[3]Section of Microbial Pathogenesis, Yale School of Medicine, New Haven, CT 06520, USA.

[4]The Howard Hughes Medical Institute, New Haven, CT 06520, USA.

Summary

During division of Gram-negative bacteria, invagination of the cytoplasmic membrane and inward growth of the peptidoglycan (PG) are followed by the cleavage of connective septal PG to allow cell separation. This PG splitting process requires temporal and spatial regulation of cell wall hydrolases. In *Escherichia coli*, LytM factors play an important role in PG splitting. Here we identify and characterize a member of this family (DipM) in *Caulobacter crescentus*. Unlike its *E. coli* counterparts, DipM is essential for viability under fast-growth conditions. Under slow-growth conditions, the Δ*dipM* mutant displays severe defects in cell division and FtsZ constriction. Consistent with its function in division, DipM colocalizes with the FtsZ ring during the cell cycle. Mutagenesis suggests that the LytM domain of DipM is essential for protein function, despite being non-canonical. DipM also carries two tandems of the PG-binding LysM domain that are sufficient for FtsZ-ring localization. Localization and fluorescence recovery after photobleaching microscopy experiments suggest that DipM localization is mediated, at least in part, by the ability of the LysM tandems to distinguish septal, multilayered PG from non-septal, monolayered PG.

Keywords

LytM; endopeptidase; peptidoglycan; localization; division; LysM

Introduction

The peptidoglycan (PG) withstands the internal osmotic pressure of bacterial cells and maintains their shape (Vollmer *et al.*, 2008a). This cell wall structure is essential for bacterial viability under most conditions, and a wide array of antibiotics target its biosynthetic pathway. In Gram-negative bacteria, the PG is thought to largely consist of a monolayer of glycan strands held together by covalently linked peptide bridges (Vollmer and Holtje, 2004). Evidence suggests that the glycan chains are oriented parallel to the cytoplasmic membrane and roughly perpendicular to the long axis of the cell (Verwer *et al.*,

* For correspondence: christine.jacobs-wagner@yale.edu Tel: 203-432-5170 Fax: 203-432-6161.
§Present address: Instituto de Investigaciones Biomedicas, Universidad Nacional Autonoma de Mexico, Mexico DF 04510.
†Present address: The Rockefeller University, New York, NY 10065.

1978; Vollmer and Holtje, 2004; Gan *et al.*, 2008). This covalently-linked network (also known as sacculus) forms a strong, elastic fabric that surrounds the cytoplasmic membrane and protects it from osmotic bursting. Peptide bridges must be cleaved to accommodate insertion of new glycan strands while preserving the integrity of the PG. This task is particularly challenging in the single layered PG of Gram-negative bacteria. Hence, PG growth requires exquisite temporal and spatial coordination between cell wall synthase and hydrolase activities.

During cell constriction, the PG grows inward concurrently with membrane invagination (Woldringh, 1976; Poindexter and Hagenzieker, 1981; Judd *et al.*, 2005), transiently forming a multilayered wall (Holtje, 1998). This process is governed by the membrane-spanning cell wall machinery that is associated with the cytokinetic FtsZ ring (den Blaauwen *et al.*, 2008; Vollmer and Bertsche, 2008). The repetition of cell wall material insertion and the pulling force generated through FtsZ ring constriction (Osawa *et al.*, 2008; Osawa *et al.*, 2009) result in inward PG growth, which is followed by degradation and release of digested PG. This key degradation process is often referred to as septal PG splitting as it cleaves the PG that links the two future daughter cells, thereby allowing outer membrane invagination and cell separation. Indeed, about 30% of the new septal PG is released during constriction (Uehara and Park, 2008).

Several cell wall enzymes such as amidases and endopeptidases have been shown to play important roles in PG splitting in *Escherichia coli* (Rodolakis *et al.*, 1973; Starka *et al.*, 1974; Heidrich *et al.*, 2001; Hara *et al.*, 2002; Heidrich *et al.*, 2002; Priyadarshini *et al.*, 2006; Priyadarshini *et al.*, 2007; Uehara *et al.*, 2009). These PG hydrolases often have redundant functions, and in most cases, single deletions of their corresponding genes have little effect on growth and division (Vollmer *et al.*, 2008b). However, inactivation of the genes encoding all three *N*-acetylmuramyl-L-alanine amidases AmiA, AmiB and AmiC results in long cell chains that are held together by connective septal cell wall (Heidrich *et al.*, 2001; Priyadarshini *et al.*, 2007). Other major players in septal PG splitting in *E. coli* include the LytM factors EnvC and NlpD. An Δ*envC* mutant forms short cell chains with regularly spaced constrictions (Rodolakis *et al.*, 1973; Hara *et al.*, 2002; Ichimura *et al.*, 2002; Bernhardt and de Boer, 2004), and this cell chaining phenotype is dramatically exacerbated when the Δ*envC* mutation is combined with a Δ*nlpD* deletion (Uehara *et al.*, 2009). While endopeptidase activity has been demonstrated for some LytM factors of Gram-positive bacteria (Browder *et al.*, 1965; Firczuk *et al.*, 2005; Cohen *et al.*, 2009; Reste de Roca *et al.*, 2010), the LytM domains of NlpD and EnvC lack some or all zinc-coordinating residues involved in catalysis. Recent evidence suggests that NlpD and EnvC do not hydrolyze the PG themselves, but rather stimulate the activity of PG amidases (Uehara *et al.*, 2010). AmiB, AmiC, EnvC and NlpD have all been shown to accumulate at the septum during *E. coli* constriction (Bernhardt and de Boer, 2003; Bernhardt and de Boer, 2004; Uehara *et al.*, 2009), consistent with an involvement in septal PG splitting. The mechanism of septal localization is, however, not well understood and is generally assumed to involve protein-protein interaction with the cell division protein complex. In the case of the amidase AmiC, this is supported with experimental evidence showing that septal localization is dependent on the late cell division protein FtsN (Bernhardt and de Boer, 2003).

Our knowledge of cell wall hydrolysis in Gram-negative bacteria is primarily limited to studies in a single model organism, *E. coli*. In this study, we identify and characterize a periplasmic LytM factor in the Gram-negative bacterium *Caulobacter crescentus*. We describe similarities to the *E. coli* paradigm as well as important differences. Additionally, we present evidence of a protein localization mechanism that relies on differential recognition of monolayered and multilayered PG.

Results

The LysM and LytM domain-containing protein DipM is involved in cell division

Since proteins belonging to the LytM family have been identified to play roles in the cell division process of *E. coli* (Bernhardt and de Boer, 2004; Uehara *et al.*, 2009), we searched the *C. crescentus* genome for proteins that contain this LytM domain. Multiple predicted proteins were identified, but one protein (CC1996) caught our attention because it contained four LysM PG-binding motifs in addition to a LytM domain (see Fig. 4A for a schematic representation of its domain organization). Further analysis of its primary sequence identified a signal peptide with a cleavage site for a signal peptidase at the N-terminus and no transmembrane-spanning segments, suggesting that CC1996 is a soluble periplasmic protein.

To characterize the function of CC1996, we created a mutant strain in which the full *cc_1996* coding sequence was substituted by an Ω spectinomycin-resistance cassette. The resulting mutant strain grew at a slower rate than the wild-type parent on PYE plates at 30°C, taking approximately twice as long to produce visible colonies. Cells from these colonies exhibited division defects (data not shown). From here on, CC1996 will be called DipM (Division Involved Protein with LysM domains). The severity of the defects associated with the Δ*dipM* mutation was dependent on growth conditions. In minimal M2G liquid medium at 30°C or below, the Δ*dipM* mutant was viable, but it was unable to propagate at 37°C in M2G liquid medium or in rich PYE liquid medium at a temperature of 30°C or above (Fig. 1A). Supplementing M2G medium with increasing amounts of rich PYE medium slowed the growth of the Δ*dipM* strain in liquid cultures (Fig. 1A). Even at 22°C, increasing concentrations of PYE in liquid M2G medium were accompanied by a dramatic enhancement of cell filamentation in the population (Fig. 1B). The morphology of wild-type cells was unaffected by such switching of growth conditions (data not shown). Collectively, our data indicate that conditions that normally increase growth rate adversely affect the ability of Δ*dipM* cells to grow and divide.

For all the following experiments, the Δ*dipM* strain was grown in M2G at 30°C. Besides the filamentation phenotype, Δ*dipM* cells tended to have short or no stalks, suggesting a potential stalk growth defect. Additionally, time-lapse microscopy of Δ*dipM* cells revealed frequent release of vesicles from the division sites (Movie S1), suggesting instability of the outer membrane at these sites. This phenotype is common among cell wall peptidase (or amidase) mutants in which the coordination between outer membrane invagination and inward PG growth has been perturbed (Rodolakis *et al.*, 1973;Heidrich *et al.*, 2001;Hara *et al.*, 2002;Heidrich *et al.*, 2002;Bernhardt and de Boer, 2004;Priyadarshini *et al.*, 2006).

Mutations in division proteins involved in cell-wall synthesis can cause altered cell pole morphologies (Taschner *et al.*, 1988; Priyadarshini *et al.*, 2006). Similarly, the poles of Δ*dipM* cells often displayed an aberrant round morphology and were frequently the widest region of the cells (Fig. 1C, black arrowheads). This was particularly striking since wild-type *C. crescentus* cells have pointed poles (Aaron *et al.*, 2007) (Fig. 1C, inset). Time-lapse microscopy of growing Δ*dipM* cells showed that the poles grow wider as they age (Movie S2), occasionally resulting in cell branching (Fig. 1C, Movie S3). These findings indicate that DipM plays an important role in cell morphogenesis.

Filamentation of ΔdipM *cells is associated with altered FtsZ dynamics*

In *E. coli*, the absence of the two main LytM factors EnvC and NlpD produces chains of cells kept together by regular septa, indicating a defect in splitting of the PG generated during cell division (Uehara *et al.*, 2009). The Δ*dipM* cell filaments were considerably different; they often displayed several constriction sites but typically at irregular intervals

(Fig. 1C, white arrow heads). To determine the degree of cytoplasmic compartmentalization in the Δ*dipM* filaments, we carried out fluorescence loss in photobleaching (FLIP) microscopy experiments. Small regions of Δ*dipM* cells producing cytoplasmic GFP were subjected to a series of photobleaching laser pulses (Figure 2A, yellow dotted regions). The extent of GFP signal loss inside the cell filaments was used as an indication of the size of the cytoplasmic compartment. We found that Δ*dipM* cell filaments had cytoplasmic compartments of sizes varying from the expected size for a normal cell to the size of an entire cell filament (Fig. 2A). Out of 104 FLIP events, 70 of them (67%) generated bleached cytoplasmic spaces much larger than normal cell size, indicating a frequent defect in cytoplasmic compartmentalization.

To better understand the Δ*dipM* filamentation phenotype, we examined FtsZ localization dynamics in growing cells by time-lapse microscopy. The FtsZ rings (labeled with FtsZ-YFP) in Δ*dipM* filaments (strain CJW3430) displayed several abnormal behaviors. Some were unstable and changed their position rapidly before completing constriction (Movie S4, arrow). Others appeared to stall or to constrict at very slow rates (Movie S4; Fig. S1, arrows). The average lifetime of FtsZ rings that eventually resulted in division was 80 ± 8 min and 140 ± 28 min for the wild-type and Δ*dipM* mutant strains (n = 20 in both cases), respectively. Occasionally, an aggregation of FtsZ-YFP signal was visible for extended periods of time (Fig. S1, line) before condensing into a ring (Fig. S1, arrowhead). Some FtsZ rings were able to complete their constriction and reassemble at other locations well before cell separation occurred (Movie S5). A possible explanation for this disconnection is that the splitting of the PG synthesized by the divisome was considerably delayed and occurred after the FtsZ ring had finished constricting and had reformed elsewhere. Close coordination between constriction of the FtsZ ring and constriction of the cell was only observed in rare cases (data not shown) and even then, the process took an unusual long time.

In *E. coli*, mutants of proteins involved in PG splitting tend to accumulate PG material at potential division sites (Priyadarshini *et al.*, 2007; Uehara *et al.*, 2009). These PG accumulations can be observed in uranyl acetate-stained EM preparations of purified sacculi and are referred to as PG rings (PeptidoGlycan) when no constriction is evident or SP rings (Septum Peptidoglycan) when constriction is visible (Priyadarshini *et al.*, 2007). Consistent with DipM playing a role in PG hydrolysis at division, both types of rings were observed in purified Δ*dipM* sacculi (Fig. 2B, arrowheads and arrows indicate PG and SP rings, respectively). No such rings were observed in sacculi of dividing wild-type cells or in sacculi of filamentous FtsZ or FtsA-depleted cells (Fig. 2B). These results suggest that DipM is involved in splitting the PG during division.

An intriguing observation in the Δ*dipM* cell filaments was the frequent relocation of the FtsZ ring before completion of constriction (Movies S4 and S5). In *C. crescentus*, the positioning of the FtsZ ring is determined by bipolar gradients of the FtsZ assembly inhibitor MipZ that form after segregation of the chromosome partitioning complex (Thanbichler and Shapiro, 2006). We hypothesized that the impairment in FtsZ ring constriction in Δ*dipM* cells may allow time for the next round of replication and segregation of the chromosomal partitioning complex. This would result in MipZ localizing at these slowly constricting or halted FtsZ rings, causing their disassembly and relocation to another division site. This idea was supported by time-lapse microscopy of FtsZ-YFP and MipZ-CFP in Δ*dipM* cells, which showed MipZ-CFP moving to the location of FtsZ ring and causing their disappearance (Fig. 2C).

Together, our observations show that in the absence of DipM, the ability of the FtsZ rings to constrict is frequently impeded, probably by an alteration in PG splitting. These stalled and

slowly constricting FtsZ rings then become susceptible to disassembly by MipZ bound to partitioning complexes before completion of cell constriction, contributing to the observed Δ*dipM* division phenotype.

DipM localizes near midcell and at the base of the stalk at specific stages of the cell cycle

Next, we examined the localization of a functional DipM-mCherry construct produced in place of DipM under native expression conditions. Time-lapse microscopy of cell cycle-synchronized populations showed early localization of the fusion protein at the old pole where a stalk later formed (Fig. 3A and Movie S6). In the stalked cell stage, DipM-mCherry formed a band near midcell while maintaining an old-pole accumulation. DipM-mCherry retained the medial localization throughout the cell constriction process until cell separation occurred. This pattern is consistent with the localization of CC1996 (now DipM) in asynchronous populations as reported in a recent proteome-wide study (Werner *et al.*, 2009). Interestingly, the old-pole accumulation of DipM-mCherry disappeared during the late cell cycle stages (Figure 3A) and did not reappear during the cell cycle of the stalked progeny (Movie S6) despite continued growth of the stalk, raising the possibility of an early role for DipM in stalk generation. A summary of DipM localization during the cell cycle is depicted in Fig. 3B.

Co-visualization of DipM-mCherry and FtsZ-YFP showed that DipM localized to the FtsZ ring position about 15 to 20 min after FtsZ ring formation and 20 min before cell constriction could be detected (Fig. 3C; under these conditions, the cell cycle is about 120 min), indicating an early localization to the FtsZ ring. In *E. coli*, FtsA and ZipA are the first known proteins to be recruited to the FtsZ ring and are required for the recruitment of other division proteins (Adams and Errington, 2009). No ZipA homolog has yet been described for *C. crescentus* but FtsA has been shown to localize early to the FtsZ ring and to be essential for division (Ohta *et al.*, 1997;Martin *et al.*, 2004). Time-lapse microscopy of DipM-mCherry and FtsZ-YFP in FtsA-depleted cell filaments revealed that DipM-mCherry colocalized with the non-constricting FtsZ-YFP rings and followed FtsZ-mYFP after disassembly and reassembly at other locations (Fig. 3D), suggesting that DipM localization to FtsZ rings is independent of FtsA. DipM-mCherry also formed bands (rings) in an *ftsA* temperature-sensitive strain at the restrictive temperature (data not shown). In *C. crescentus*, MreB also displays an early recruitment to the FtsZ ring and this recruitment is prevented by a Q26P substitution in MreB (Aaron *et al.*, 2007). In an $mreB_{Q26P}$ background, DipM-mCherry localization near midcell was retained (Fig. 3E), suggesting that DipM localization to the FtsZ ring is also MreB-independent. Not surprisingly, however, DipM localization was dependent on FtsZ as DipM-mCherry failed to form bands in FtsZ-depleted cells (Fig. 3F).

The N-proximal tandem of LysM domains is necessary and largely sufficient for DipM localization

In order to determine the region(s) of DipM required for its localization, we generated a series of protein truncations fused to mCherry. These fusions (with the exception of the one shown in Fig. 4B, i, which was produced from the native promoter) were produced from the chromosome under the control of the vanillate-inducible promoter (*vanAp*) in an otherwise wild-type *dipM* background. We verified the size and integrity of the fusions by Western blot analysis (Fig. S2)

The DipM protein can be divided into three regions based on its domain composition (Fig. 4A): an N-terminal region carrying two neighboring PG-binding LysM motifs, a central region carrying two more adjacent LysMs and a C-terminal region containing the predicted LytM peptidase domain. The region containing the LytM domain was dispensable for

localization (see localization of DipM$_{\Delta 501\text{-}609}$-mCherry; Fig. 4B, ii). The absence of the N-terminal region carrying the first LysM tandem abolished almost all localization (mCherry-DipM$_{\Delta 1\text{-}236}$; Fig.4B, vii). Conversely, the N-terminal region with the first LysM tandem alone displayed a slightly weaker, but otherwise normal localization pattern even in the absence of the second LysM tandem and LytM domain (DipM$_{\Delta 297\text{-}609}$-mCherry; Fig. 4B, iii). The presence of two LysMs in tandem was critical for localization as an in-frame deletion of either LysM motif within the tandem (DipM$_{1\text{–}296\Delta 121\text{–}167}$-mCherry and DipM$_{1\text{–}296\Delta 175\text{–}223}$-mCherry) resulted in dispersed localization in the periplasm (Fig. 4, iv and v, respectively). Since the first and second proline-rich linkers were preserved in these constructs, these results indicate that these linkers are not important for localization; instead they argue that the N-proximal tandem of LysM domains is the major cis-acting determinant of localization.

The LysM domains of DipM can differentiate between two types of peptidoglycan

The LysM domain is a widespread protein module that binds PG (Buist *et al.*, 2008) and a recent atomic force microscopy study has demonstrated that the LysM-PG interaction occurs with high affinity and specificity (Andre *et al.*, 2008). Many LysM-containing proteins are cell-wall hydrolases and by binding to PG, the LysM domains are thought to increase the local concentration of the enzyme, bring the catalytic domain closer to its substrate, and/or help the enzyme slide along the polymeric PG (Steen *et al.*, 2005). DipM has a predicted LytM peptidase domain at its C-terminus. This LytM domain, while dispensable for localization (Fig. 4B, ii), was required for DipM function. This was shown by producing the localization-proficient DipM$_{\Delta 501\text{-}609}$-mCherry construct (carrying the two LysM tandems but lacking the LytM domain) in cells in which wild-type *dipM* is under vanillate-controlled expression (strain CJW3122). Cells had a normal morphology in the presence of vanillic acid, but repression of wild-type *dipM* expression after removal of vanillic acid from the culture medium resulted in cell filamentation characteristic of the DipM$^-$ phenotype (Fig. 5A). Interestingly, in these DipM-depleted cells, the localization-proficient DipM$_{\Delta 501\text{-}609}$-mCherry fusion not only accumulated in bands, as we would expect for filamentous cells that form FtsZ rings (e.g., see DipM localization in FtsA-depleted cells; Fig. 3D), but also accumulated over wide regions along the cell filaments (Fig. 5A). These accumulations were not the result of an uneven periplasmic volume along the cell filaments, as demonstrated by the largely dispersed distribution of freely diffusible mCherry in the periplasm of Δ*dipM* cells (Fig. S3). Moreover, freely diffusible, periplasmic mCherry molecules were clearly present in the outer membrane vesicles shed by the Δ*dipM* mutant, unlike the DipM$_{\Delta 501\text{-}609}$-mCherry construct, consistent with the later binding to the PG through its LysM domains.

We considered the possibility that the widespread accumulations of DipM$_{\Delta 501\text{-}609}$-mCherry in DipM$^-$ cells might be caused by the presence of specific PG material that is temporarily left behind in the absence of DipM activity, to which the LysM domains of DipM have a higher binding affinity. To test this idea, we carried out fluorescence recovery after photobleaching (FRAP) experiments. As expected for freely diffusing molecules, a periplasmic mCherry fusion displayed fast kinetics of fluorescence recovery after photobleaching that were not significantly different in DipM- and FtsZ-depleted cells (data not shown). In contrast, we observed no detectable recovery of DipM$_{\Delta 501\text{-}609}$-mCherry fluorescence over 10 min within the photobleached regions (Fig. 5B; n=21 cells). This is consistent with the LysM tandems of DipM strongly binding to the PG of Δ*dipM* cells, virtually eliminating protein mobility. On the other hand, in FtsZ-depleted cells where no septal PG is present and DipM has an uniform spatial distribution, recovery of DipM$_{\Delta 501\text{-}609}$-mCherry signal within photobleached regions occurred at a detectable rate (Fig. 5B, n=20 cells) with a recovery half-time of 13.6 s (±4.6 s). In the absence of fluorescence recovery in the DipM-depleted cells, we could not calculate a recovery half-

time value for DipM$_{\Delta 501\text{-}609}$-mCherry for quantitative comparison. Therefore, to reduce binding to the PG and thereby increase mobility in the periplasm, we performed FRAP experiments with a mCherry reporter construct that contains only one LysM tandem (instead of two) in DipM-depleted and FtsZ-depleted cells. Mobility of this construct (DipM$\Delta_{297\text{-}609}$-mCherry) was increased in both backgrounds (Fig. 5C), consistent with our interpretation that PG binding through the LysM domains largely accounts for the restricted mobility. Perhaps more importantly, fluorescence recovery was much faster in the FtsZ-depleted cells, with estimated recovery half-times of 1.1 s (±0.271 s) and 17.6 s (±1.7 s) in FtsZ-depleted and DipM-depleted cells, respectively (Fig. 5C). Thus, there is about a 16-fold difference in mobility for a construct with a single LysM tandem. Although the second LysM tandem cannot localize by itself, the observation that in conjunction with the first tandem, protein localization is enhanced (Fig. 4B, ii versus iii) suggests that the difference in binding selectivity could be even larger when two LysM tandems are present.

Taken together, these results suggest that localization of DipM is mediated by the discriminating specificity of LysM tandems for different types of PG.

The non-canonical LytM domain of DipM is required for protein function

The C-terminal region carrying the LytM domain of DipM is dispensable for localization (Fig. 4B, ii) but is essential for DipM function (Fig. 5A), consistent with a role in PG splitting during constriction. LytM domains have been shown to have metallo-endopeptidase activity in Gram-positive bacteria (Ramadurai *et al.*, 1999; Horsburgh *et al.*, 2003). The crystal structure of *Staphylococcus aureus* LytM identifies three conserved amino acids that directly coordinate zinc (Odintsov *et al.*, 2004; Firczuk *et al.*, 2005). Only one of these residues is conserved in DipM (H585; Fig. 6A). The other two amino acids are substituted by asparagines (N503 and N507, Fig. 6A), which, at least in principle, can coordinate zinc (Harding, 2004; Passerini *et al.*, 2007).

To examine whether the LytM domain alone can support protein function, we generated two additional mCherry fusions, one to the full-length DipM protein (DipM-mCherry) and the other to the LytM domain alone (DipM$_{\Delta 54\text{-}419}$-mCherry). The synthesis of these fusions was then induced from the vanillic acid-inducible promoter on a low-copy copy plasmid (pRVCHYC-2) in a Δ*dipM* background. The minimal concentration of inducer (vanillic acid) needed to obtain full complementation of the Δ*dipM* filamentation phenotype with the wild-type DipM-mCherry construct was 15 μM (Fig. 6B). Consistent with the notion that the non-canonical LytM domain is required for function, expression of DipM$_{\Delta 54\text{-}419}$-mCherry partially suppressed the Δ*dipM* filamentation phenotype (Fig. 6C), especially when overexpressed (i.e., in the presence of 250 μM of inducer).

As expected, this DipM$_{\Delta 54\text{-}419}$-mCherry fusion lacking the LysM tandems displayed a largely uniform fluorescent signal, except for a slightly brighter signal at deeply constricted sites on rare occasions (Fig. 6C, arrow). These small accumulations of signal are possibly caused by a local increase in periplasmic volume due to outer membrane instability, as observed for the freely diffusing periplasmic mCherry (Fig. S3) and as suggested previously for the *envC* mutant (Bernhardt and de Boer, 2004). The defect in localization was not due to mCherry being cleaved off from the fusion as verified by Western blot (Fig. S2). Importantly, the suppression of the Δ*dipM* filamentation phenotype by the LytM domain alone remained only partial even when it was overproduced (in the presence of 250 μM of inducer; Fig. 6C). This demonstrates the importance of positioning the LytM domain activity at the correct cellular locations.

Discussion

Cell wall proteins including the LytM factors have been proposed to play a crucial role in cell division by separating or promoting the separation of the interlinked PG of daughter cells (Rodolakis *et al.*, 1973; Starka *et al.*, 1974; Lange and Hengge-Aronis, 1994; Heidrich *et al.*, 2001; Hara *et al.*, 2002; Bernhardt and de Boer, 2004; Garcia and Dillard, 2006; Priyadarshini *et al.*, 2006; Uehara *et al.*, 2009; Uehara *et al.*, 2010). In this study, we identify DipM, a protein with a non-canonical LytM domain that has a similar role in PG splitting in *C. crescentus.* Consistent with this function, DipM is a periplasmic protein that localizes to the future site of division in *C. crescentus* (Fig. 3A-C) and while its function is dispensable for viability under slow growth conditions (e.g., low temperature or low-nutrient medium), it is essential for viability under fast growing conditions (Fig. 1A). This indicates that although some functional redundancy exists, this redundancy is not sufficient to sustain rapid cell multiplication. Even under slow-growth conditions, DipM function is very important as Δ*dipM* cells display severe cell division defects with a large fraction of the population forming long filaments that occasionally divide. These Δ*dipM* cell filaments are constricted at irregular intervals (Fig. 1C), unlike the chain-forming mutants in *E. coli* (Heidrich *et al.*, 2001; Uehara *et al.*, 2009). This cell filamentation phenotype is in part due to a de-synchronization between the progression of cell division and segregation of the partition complex, causing the disassembly of FtsZ rings by the partitioning complex-associated protein MipZ (Fig. 2C). A similar effect is observed under conditions in which recruitment of septal proteins (such as MurG and PBP3) to the FtsZ ring is considerably impaired (Y. Tsuge, G. Ebersbach and C. Jacobs-Wagner, unpublished results). Desynchronization between cytokinesis and segregation of the DNA partition complex in Δ*dipM* cells seems to be caused by an apparent stalling or slower constriction of the FtsZ ring (Movies S4 and S5; Fig. S1). A defect in FtsZ ring constriction also appears to occur in *E. coli* when the LytM factor EnvC is absent (Hara *et al.*, 2002). Interestingly, a mutation in the *envC* gene causes a synthetic sick phenotype when combined with a deletion of the *minCDE* operon (Bernhardt and de Boer, 2004), and MinD is a functional homolog of MipZ.

How could DipM affect FtsZ ring constriction? Cell division in Gram-negative bacteria involves the invagination of three cell layers: the cytoplasmic membrane, the PG and the outer membrane. The cytoplasmic membrane maintains a close association with the outer membrane and the growing PG through the cell division protein complex (MacAlister *et al.*, 1987; Gerding *et al.*, 2007). A possible reason for the slowdown in FtsZ ring constriction in Δ*dipM* cells may involve the loss of contact between the cytoplasmic and outer membranes, as coordinated invagination of the cytoplasmic and outer membranes (Poindexter and Hagenzieker, 1981; Judd *et al.*, 2005) requires proper splitting of the growing PG. The shedding of vesicles at division sites in the Δ*dipM* mutant (Movie S1) is consistent with loss of interaction between the outer membrane and the other two layers (Knox *et al.*, 1966; Deatherage *et al.*, 2009). Another, perhaps more attractive possibility by which DipM affects FtsZ ring constriction relates more directly to its function in splitting FtsZ-ring-directed peptidoglycan. In *E. coli*, cleavage of septal PG during constriction is accompanied by the release of PG fragments (Uehara and Park, 2008). In the absence of DipM, other hydrolysis-inducing activities can partially take over at least under slow-growth rate conditions, but their activity may not be as selective and they may also cause the cleavage of peptide bonds involved in inward PG growth, causing it to stall or even rescind. While FtsZ rings can generate force by themselves in tubular liposomes (Osawa *et al.*, 2008), recent theoretical calculations suggest that inward PG growth can help the progressivity of FtsZ ring constriction (Lan *et al.*, 2009). The frequent stalling (Fig. 1S) and occasional rescinding (Movie S1) of FtsZ ring constriction in Δ*dipM* cells are consistent with this notion.

Similarly to DipM, the two main LytM factors involved in septal PG splitting in *E. coli*, EnvC and NlpD (Uehara *et al.*, 2009), have non-conserved amino acids at the metal-coordinating positions (Ichimura *et al.*, 2002). It was recently shown that theses two proteins do not hydrolyze the PG but instead acts as activators of PG amidases (Uehara *et al.*, 2010). It is possible that DipM has a similar regulatory function, although the LytM domain of DipM is essential for function and is sufficient to partially suppress the Δ*dipM* phenotype when overexpressed (Fig. 6). Future work will be required to determine the specific role of DipM LytM domain in PG splitting.

In *C. crescentus*, the FtsZ ring, which forms well before initiation of cell constriction, directs PG synthesis, not only during division, but also during a large portion of the cell elongation phase (Aaron *et al.*, 2007). DipM is recruited relatively early to the FtsZ ring location well before cell constriction becomes discernible (Fig. 3C), suggesting a possible early role in FtsZ-ring-directed PG synthesis. Our data suggest that localization occurs, at least in part, through the preferential binding of the LysM tandems of DipM to the FtsZ ring-directed PG. In the absence of DipM activity, a DipM construct carrying the LysM tandems (but not the LytM domain) accumulates not only in bands at presumed FtsZ ring locations, but also in large adjacent regions (Fig. 5A). FRAP experiments suggest that these regions contain PG for which the DipM LysM domains have higher binding affinity (Fig. 5B-C). We envision that these regions correspond to multilayered PG synthesized by the FtsZ-associated cell wall enzymes. FtsZ-directed PG growth temporarily generates multilayered PG that is progressively removed by cell wall hydrolases. Our findings suggest that DipM greatly contributes to such activity by mediating –directly or indirectly– the selective cleavage of the crosslinks most distal from the cytoplasmic membrane and that DipM accumulates where it is needed through preferential binding of its LysM tandems to multilayered PG rather than monolayered PG. This idea predicts that the absence of DipM would result in accumulation of multiple layers of glycan strands at existing and former FtsZ ring positions, which is consistent with the formation of PG- and SP-rings in Δ*dipM* cell filaments (Fig. 2B). Similarly, the frequent instability of the FtsZ ring in the Δ*dipM* background (Fig. S1, lines and Movie S4) would cause the accumulation of glycan strands over wide regions, thereby generating large patches of multilayered PG throughout the length of Δ*dipM* cell filaments. Consistent with this, cryo-electron tomography of Δ*dipM* sacculi reveals notable thickening of PG throughout the mutant sacculi (Goley et al., in press), in good agreement with the localization pattern and the FRAP analysis of the inactive, localization-proficient LysM-containing constructs in the Δ*dipM* mutant (Fig. 5).

How would the LysM domains of DipM recognize multilayered PG over the more common monolayered form? Structural and biochemical studies reveal that LysM domains bind to the *N*-acetylglucosamine moiety of the PG (Buist *et al.*, 2008). DipM contains two LysM tandems (Fig. 4A) and the N-proximal LysM tandem is sufficient to mediate septal localization (Fig. 4iii), although not as strongly as when it is connected to the second LysM tandem (Fig. 4ii). It was recently shown in vitro that a single LysM domain of *Pteris ryukyuensis* Chitinase A binds to glycan chains of four *N*-acetylglucosamine residues in a 1:1 ratio, whereas a tandem of this LysM domain binds to these glycan chains in a 1:2 ratio (Ohnuma *et al.*, 2008). These stoichiometries suggest the possibility that each LysM tandem of DipM binds to two adjacent glycan strands. In the regular monolayered PG, adjacent glycan strands are connected by peptide bridges that are stretched by the turgor pressure (Oldmixon *et al.*, 1974; Koch, 2000). In contrast, in the multilayered, septal PG, the underlying glycan strands are connected with each other and with the stress-bearing layer by peptide bridges that are in a relaxed state. Accordingly, the glycan strands are closer to each other when the peptide cross-links are relaxed, perhaps allowing the simultaneous binding of the two LysM domains in the tandem to adjacent glycan strands. Conversely, adjacent glycan strands connected with stretched peptides (as in the stress-bearing, monolayered PG)

may be too far apart, allowing only one of the LysM domains of the tandem to bind at a time, reducing the binding strength, which would be consistent with our FRAP measurements (Fig. 5B-C). Turgor pressure is also thought to produce a conformational change in the stress-bearing glycan chains (from straight to a tessera conformation) by changing the relative orientation of the disaccharides (Koch, 1998; Ursinus *et al.*, 2004; Vollmer and Seligman, 2010). Therefore, an alternative hypothesis for the septal localization of DipM may involve the relaxation state of the glycan strands rather than that of the peptide cross-links. It is formally possible that the LysM domains in tandem bind to *N*-acetylglucosamine residues of the same glycan strand and that the spacing and arrangement between *N*-acetylglucosamines might be more favorable for the binding of both LysM motifs of each tandem when the glycan strands are in a relaxed state. In either scenario, DipM would preferentially bind to the underlying, unstressed glycan strands and thereby localize to the multilayered FtsZ-directed PG by distinguishing a physical difference in PG. We also cannot rule out the possibility that the multilayered PG presents a chemical difference for which the LysM tandem has a higher affinity. This would be reminiscent of the proposed localization mechanism for FtsN and other SPOR-containing proteins (Ursinus *et al.*, 2004; Yang *et al.*, 2004; Mishima *et al.*, 2005; Gerding *et al.*, 2009; Lutkenhaus, 2009). Localization of these proteins to the septum is mediated by their SPOR domain, which preferentially binds to PG glycan strands stripped of peptide chains. Differential recognition of PG forms by PG-binding domains may thus represent an effective strategy for spatial and temporal regulation of cell wall activities.

Experimental procedures

Strains and culture conditions

All *C. crescentus* cultures were grown in liquid M2G medium or on solid PYE-agar medium at 30°C (Ely, 1991), unless otherwise indicated. *E. coli* strains were grown in LB broth. Antibiotics for *C. crescentus* were used at the following final concentrations (in μg/ml) for liquid and solid media correspondingly: Gentamycin, 2 and 5; kanamycin, 5 and 20; oxytetracycline, 1 and 2; spectinomycin, 25 and 100; apramycin 8. For *E. coli*, the following concentrations (in μg/ml) were used for liquid and solid media: Ampicillin, 150 and 200; gentamycin, 10 and 20; kanamycin, 50; oxytetracycline, 20; spectinomycin, 50. The strains and plasmids used in this study are listed in Tables 1 and 2, respectively. Their construction is described in the supplementary text.

Microscopy and analysis

Light microscopy images were obtained using a Nikon E1000 or NIKON E80i equipped with a Hamamatsu ORCA ER camera or a NIKON E80i equipped with an Andor iXon^{EM}+ CCD camera. Cells were grown to an OD_{660} between 0.2 and 0.3, and immobilized on agarose-padded slides containing M2G medium for imaging at room temperature. Images were taken and processed with Metamorph 7.1.4 software or ImageJ. Cell size measurements were performed as described (Angelastro *et al.*, 2009). For the FLIP experiments, a Photonic Instrument Micropoint Laser system was used with a 481-nm Laser Dye, set at 15 pulses with a power of 2 at the attenuator plate and 20 for the internal attenuator. For the FRAP experiments, a 552-nm Laser Dye was used set at 8 or 2 pulses with a power of 1 and 40 for the internal attenuator. For both FLIP and FRAP experiments the laser intensity was cut by 70% through a beam splitter, and attenuated 4X by a neutral density filter. The fluorescence recovery data was processed in Microsoft Excel. Fitting was achieved using the MATLAB “cftool” application and function $F(t)=A(1-e^{-bt})$ where F, t, A, and b are fluorescence intensity, time, maximal recovery fluorescence, and recovery rate, respectively.

Electron microscopy

A diluted suspension of purified sacculi was spotted for 15 min on Carbon-B coated Formvar 200 mesh copper grids (TedPella) that had been previously air-ionized for 30 s. The grids were then washed with water and stained for 10 min with a 3% uranyl acetate solution, washed again and allowed to dry. Imaging was carried out on a Jeol JEM-1230 transmission electron microscope operating at 80 kV. Digital images were acquired with a Hamamatsu ORCA-HR camera. SEM images were obtained as described previously (Takacs *et al*. 2010).

Molecular biology techniques and Western blot

For PCR reactions, the TaKaRa PrimeSTAR-HS DNA polymerase was used as directed by the manufacturer. DNA restriction and ligase reactions were carried out with enzymes from New England BioLabs. Immunoblots were done using standard techniques and an anti-RFP antibody.

Supplementary Material

Refer to Web version on PubMed Central for supplementary material.

Acknowledgments

The authors wish to thank the Jacobs-Wagner lab members for helpful discussion and critical reading of the manuscript, and L. Shapiro for the anti-RFP antibody. We also thank L. Shapiro, M. Thanbichler and their colleagues for agreeing on the DipM name. This work was supported by the National Institutes of Health (GM076698 and GM065835 to C.J-W.), the European Commission within the EUR-INTAFAR project (to W.V.) and the Howard Hughes Medical Institute (to C.J-W.). S.P. was supported in part by a PEW Latin American fellowship and C.N.T. was supported in part by a Yale College Dean's Office Science, Technology and Research Scholars (STARS) II fellowship.

References

Aaron M, Charbon G, Lam H, Schwarz H, Vollmer W, Jacobs-Wagner C. The tubulin homologue FtsZ contributes to cell elongation by guiding cell wall precursor synthesis in *Caulobacter crescentus*. Mol Microbiol. 2007; 64:938–952. [PubMed: 17501919]

Adams DW, Errington J. Bacterial cell division: assembly, maintenance and disassembly of the Z ring. Nat Rev Microbiol. 2009; 7:642–653. [PubMed: 19680248]

Andre G, Leenhouts K, Hols P, Dufrene YF. Detection and localization of single LysM-peptidoglycan interactions. J Bacteriol. 2008; 190:7079–7086. [PubMed: 18757536]

Angelastro PS, Sliusarenko O, Jacobs-Wagner C. Polar localization of the CckA histidine kinase and cell cycle periodicity of the essential master regulator CtrA in *Caulobacter crescentus*. J Bacteriol. 2009

Bernhardt TG, de Boer PA. The *Escherichia coli* amidase AmiC is a periplasmic septal ring component exported via the twin-arginine transport pathway. Mol Microbiol. 2003; 48:1171–1182. [PubMed: 12787347]

Bernhardt TG, de Boer PA. Screening for synthetic lethal mutants in *Escherichia coli* and identification of EnvC (YibP) as a periplasmic septal ring factor with murein hydrolase activity. Mol Microbiol. 2004; 52:1255–1269. [PubMed: 15165230]

Browder HP, Zygmunt WA, Young JR, Tavormina PA. Lysostaphin: Enzymatic Mode of Action. Biochem Biophys Res Commun. 1965; 19:383–389. [PubMed: 14317407]

Buist G, Steen A, Kok J, Kuipers OP. LysM, a widely distributed protein motif for binding to (peptido)glycans. Mol Microbiol. 2008; 68:838–847. [PubMed: 18430080]

Cohen DN, Sham YY, Haugstad GD, Xiang Y, Rossmann MG, Anderson DL, Popham DL. Shared catalysis in virus entry and bacterial cell wall depolymerization. J Mol Biol. 2009; 387:607–618. [PubMed: 19361422]

Deatherage BL, Lara JC, Bergsbaken T, Rassoulian Barrett SL, Lara S, Cookson BT. Biogenesis of bacterial membrane vesicles. Mol Microbiol. 2009; 72:1395–1407. [PubMed: 19432795]

den Blaauwen T, de Pedro MA, Nguyen-Disteche M, Ayala JA. Morphogenesis of rod-shaped sacculi. FEMS Microbiol Rev. 2008; 32:321–344. [PubMed: 18291013]

Ely B. Genetics of *Caulobacter crescentus*. Methods Enzymol. 1991; 204:372–384. [PubMed: 1658564]

Evinger M, Agabian N. Envelope-associated nucleoid from *Caulobacter crescentus* stalked and swarmer cells. J Bacteriol. 1977; 132:294–301. [PubMed: 334726]

Firczuk M, Mucha A, Bochtler M. Crystal structures of active LytM. J Mol Biol. 2005; 354:578–590. [PubMed: 16269153]

Gan L, Chen S, Jensen GJ. Molecular organization of Gram-negative peptidoglycan. Proc Natl Acad Sci U S A. 2008; 105:18953–18957. [PubMed: 19033194]

Garcia DL, Dillard JP. AmiC functions as an *N*-acetylmuramyl-l-alanine amidase necessary for cell separation and can promote autolysis in *Neisseria gonorrhoeae*. J Bacteriol. 2006; 188:7211–7221. [PubMed: 17015660]

Gerding MA, Liu B, Bendezu FO, Hale CA, Bernhardt TG, de Boer PA. Self-enhanced accumulation of FtsN at division sites, and roles for other proteins with a SPOR domain (DamX, DedD, and RlpA) in *Escherichia coli* cell constriction. J Bacteriol. 2009

Gerding MA, Ogata Y, Pecora ND, Niki H, de Boer PA. The trans-envelope Tol-Pal complex is part of the cell division machinery and required for proper outer-membrane invagination during cell constriction in *E. coli*. Mol Microbiol. 2007; 63:1008–1025. [PubMed: 17233825]

Hara H, Narita S, Karibian D, Park JT, Yamamoto Y, Nishimura Y. Identification and characterization of the *Escherichia coli envC* gene encoding a periplasmic coiled-coil protein with putative peptidase activity. FEMS Microbiol Lett. 2002; 212:229–236. [PubMed: 12113939]

Harding MM. The architecture of metal coordination groups in proteins. Acta Crystallogr D Biol Crystallogr. 2004; 60:849–859. [PubMed: 15103130]

Heidrich C, Templin MF, Ursinus A, Merdanovic M, Berger J, Schwarz H, de Pedro MA, Holtje JV. Involvement of *N*-acetylmuramyl-L-alanine amidases in cell separation and antibiotic-induced autolysis of *Escherichia coli*. Mol Microbiol. 2001; 41:167–178. [PubMed: 11454209]

Heidrich C, Ursinus A, Berger J, Schwarz H, Holtje JV. Effects of multiple deletions of murein hydrolases on viability, septum cleavage, and sensitivity to large toxic molecules in *Escherichia coli*. J Bacteriol. 2002; 184:6093–6099. [PubMed: 12399477]

Holtje JV. Growth of the stress-bearing and shape-maintaining murein sacculus of *Escherichia coli*. Microbiol Mol Biol Rev. 1998; 62:181–203. [PubMed: 9529891]

Horsburgh GJ, Atrih A, Foster SJ. Characterization of LytH, a differentiation-associated peptidoglycan hydrolase of *Bacillus subtilis* involved in endospore cortex maturation. J Bacteriol. 2003; 185:3813–3820. [PubMed: 12813075]

Ichimura T, Yamazoe M, Maeda M, Wada C, Hiraga S. Proteolytic activity of YibP protein in *Escherichia coli*. J Bacteriol. 2002; 184:2595–2602. [PubMed: 11976287]

Judd EM, Comolli LR, Chen JC, Downing KH, Moerner WE, McAdams HH. Distinct constrictive processes, separated in time and space, divide *Caulobacter* inner and outer membranes. J Bacteriol. 2005; 187:6874–6882. [PubMed: 16199556]

Knox KW, Vesk M, Work E. Relation between excreted lipopolysaccharide complexes and surface structures of a lysine-limited culture of *Escherichia coli*. J Bacteriol. 1966; 92:1206–1217. [PubMed: 4959044]

Koch AL. Orientation of the peptidoglycan chains in the sacculus of Escherichia coli. Res Microbiol. 1998; 149:689–701. [PubMed: 9921576]

Koch AL. Simulation of the conformation of the murein fabric: the oligoglycan, pentamuropeptide, and cross-linked nona-muropeptide. Arch Microbiol. 2000; 174:429–439. [PubMed: 11195099]

Lan G, Daniels BR, Dobrowsky TM, Wirtz D, Sun SX. Condensation of FtsZ filaments can drive bacterial cell division. Proc Natl Acad Sci U S A. 2009; 106:121–126. [PubMed: 19116281]

Lange R, Hengge-Aronis R. The *nlpD* gene is located in an operon with *rpoS* on the *Escherichia coli* chromosome and encodes a novel lipoprotein with a potential function in cell wall formation. Mol Microbiol. 1994; 13:733–743. [PubMed: 7997184]

Lutkenhaus J. FtsN - trigger for septation. J Bacteriol. 2009

MacAlister TJ, Cook WR, Weigand R, Rothfield LI. Membrane-murein attachment at the leading edge of the division septum: a second membrane-murein structure associated with morphogenesis of the gram-negative bacterial division septum. J Bacteriol. 1987; 169:3945–3951. [PubMed: 3305476]

Martin ME, Trimble MJ, Brun YV. Cell cycle-dependent abundance, stability and localization of FtsA and FtsQ in *Caulobacter crescentus*. Mol Microbiol. 2004; 54:60–74. [PubMed: 15458405]

Mishima M, Shida T, Yabuki K, Kato K, Sekiguchi J, Kojima C. Solution structure of the peptidoglycan binding domain of *Bacillus subtilis* cell wall lytic enzyme CwlC: characterization of the sporulation-related repeats by NMR. Biochemistry. 2005; 44:10153–10163. [PubMed: 16042392]

Odintsov SG, Sabala I, Marcyjaniak M, Bochtler M. Latent LytM at 1.3A resolution. J Mol Biol. 2004; 335:775–785. [PubMed: 14687573]

Ohnuma T, Onaga S, Murata K, Taira T, Katoh E. LysM domains from *Pteris ryukyuensis* chitinase-A: a stability study and characterization of the chitin-binding site. J Biol Chem. 2008; 283:5178–5187. [PubMed: 18083709]

Ohta N, Ninfa AJ, Allaire A, Kulick L, Newton A. Identification, characterization, and chromosomal organization of cell division cycle genes in *Caulobacter crescentus*. J Bacteriol. 1997; 179:2169–2180. [PubMed: 9079901]

Oldmixon EH, Glauser S, Higgins ML. Two proposed general configurations for bacterial cell wall peptidoglycans shown by space-filling molecular models. Biopolymers. 1974; 13:2037–2060. [PubMed: 4215473]

Osawa M, Anderson DE, Erickson HP. Reconstitution of contractile FtsZ rings in liposomes. Science. 2008; 320:792–794. [PubMed: 18420899]

Osawa M, Anderson DE, Erickson HP. Curved FtsZ protofilaments generate bending forces on liposome membranes. EMBO J. 2009; 28:3476–3484. [PubMed: 19779463]

Passerini A, Andreini C, Menchetti S, Rosato A, Frasconi P. Predicting zinc binding at the proteome level. BMC Bioinformatics. 2007; 8:39. [PubMed: 17280606]

Poindexter JS, Hagenzieker JG. Constriction and septation during cell division in caulobacters. Can J Microbiol. 1981; 27:704–719. [PubMed: 6794894]

Priyadarshini R, de Pedro MA, Young KD. Role of peptidoglycan amidases in the development and morphology of the division septum in *Escherichia coli*. J Bacteriol. 2007; 189:5334–5347. [PubMed: 17483214]

Priyadarshini R, Popham DL, Young KD. Daughter cell separation by penicillin-binding proteins and peptidoglycan amidases in *Escherichia coli*. J Bacteriol. 2006; 188:5345–5355. [PubMed: 16855223]

Ramadurai L, Lockwood KJ, Nadakavukaren MJ, Jayaswal RK. Characterization of a chromosomally encoded glycylglycine endopeptidase of *Staphylococcus aureus*. Microbiology. 1999; 145(Pt 4): 801–808. [PubMed: 10220159]

Reste de Roca F, Duche C, Dong S, Rince A, Dubost L, Pritchard DG, Baker JR, Arthur M, Mesnage S. Cleavage Specificity of *Enterococcus faecalis* EnpA (EF1473), a Peptidoglycan Endopeptidase Related to the LytM/Lysostaphin Family of Metallopeptidases. J Mol Biol. 2010

Rodolakis A, Thomas P, Starka J. Morphological mutants of *Escherichia coli*. Isolation and ultrastructure of a chain-forming *envC* mutant. J Gen Microbiol. 1973; 75:409–416. [PubMed: 4574921]

Starka J, Di Savino D, Michel G, Rodolakis A, Thomas P. Phenotypic expression of an *envC*-division mutant of *Escherichia coli* K12. Ann Microbiol (Paris). 1974; 125 B:227–232. [PubMed: 4218460]

Steen A, Buist G, Horsburgh GJ, Venema G, Kuipers OP, Foster SJ, Kok J. AcmA of *Lactococcus lactis* is an *N*-acetylglucosaminidase with an optimal number of LysM domains for proper functioning. FEBS J. 2005; 272:2854–2868. [PubMed: 15943817]

Takacs CN, Poggio S, Charbon G, Pucheault M, Vollmer W, Jacobs-Wagner C. MreB drives de novo rod morphogenesis in *Caulobacter crescentus* via remodeling of the cell wall. J Bacteriol. 2010; 192:1671–1684. [PubMed: 20023035]

Taschner PE, Ypenburg N, Spratt BG, Woldringh CL. An amino acid substitution in penicillin-binding protein 3 creates pointed polar caps in *Escherichia coli*. J Bacteriol. 1988; 170:4828–4837. [PubMed: 3049550]

Thanbichler M, Iniesta AA, Shapiro L. A comprehensive set of plasmids for vanillate- and xylose-inducible gene expression in *Caulobacter crescentus*. Nucleic Acids Res. 2007; 35:e137. [PubMed: 17959646]

Thanbichler M, Shapiro L. MipZ, a spatial regulator coordinating chromosome segregation with cell division in *Caulobacter*. Cell. 2006; 126:147–162. [PubMed: 16839883]

Uehara T, Dinh T, Bernhardt TG. LytM-domain factors are required for daughter cell separation and rapid ampicillin-induced lysis in *Escherichia coli*. J Bacteriol. 2009; 191:5094–5107. [PubMed: 19525345]

Uehara T, Park JT. Growth of *Escherichia coli*: significance of peptidoglycan degradation during elongation and septation. J Bacteriol. 2008; 190:3914–3922. [PubMed: 18390656]

Uehara T, Parzych KR, Dinh T, Bernhardt TG. Daughter cell separation is controlled by cytokinetic ring-activated cell wall hydrolysis. EMBO J. 2010

Ursinus A, van den Ent F, Brechtel S, de Pedro M, Holtje JV, Lowe J, Vollmer W. Murein (peptidoglycan) binding property of the essential cell division protein FtsN from *Escherichia coli*. J Bacteriol. 2004; 186:6728–6737. [PubMed: 15466024]

Verwer RW, Nanninga N, Keck W, Schwarz U. Arrangement of glycan chains in the sacculus of *Escherichia coli*. J Bacteriol. 1978; 136:723–729. [PubMed: 361720]

Vollmer W, Bertsche U. Murein (peptidoglycan) structure, architecture and biosynthesis in *Escherichia coli*. Biochim Biophys Acta. 2008; 1778:1714–1734. [PubMed: 17658458]

Vollmer W, Blanot D, de Pedro MA. Peptidoglycan structure and architecture. FEMS Microbiol Rev. 2008a; 32:149–167. [PubMed: 18194336]

Vollmer W, Holtje JV. The architecture of the murein (peptidoglycan) in gram-negative bacteria: vertical scaffold or horizontal layer(s)? J Bacteriol. 2004; 186:5978–5987. [PubMed: 15342566]

Vollmer W, Joris B, Charlier P, Foster S. Bacterial peptidoglycan (murein) hydrolases. FEMS Microbiol Rev. 2008b; 32:259–286. [PubMed: 18266855]

Vollmer W, Seligman SJ. Architecture of peptidoglycan: more data and more models. Trends Microbiol. 2010; 18:59–66. [PubMed: 20060721]

Wang Y, Jones BD, Brun YV. A set of ftsZ mutants blocked at different stages of cell division in *Caulobacter*. Mol Microbiol. 2001; 40:347–360. [PubMed: 11309118]

Werner JN, Chen EY, Guberman JM, Zippilli AR, Irgon JJ, Gitai Z. Quantitative genome-scale analysis of protein localization in an asymmetric bacterium. Proc Natl Acad Sci U S A. 2009; 106:7858–7863. [PubMed: 19416866]

Woldringh CL. Morphological analysis of nuclear separation and cell division during the life cycle of *Escherichia coli*. J Bacteriol. 1976; 125:248–257. [PubMed: 1107308]

Yang JC, Van Den Ent F, Neuhaus D, Brevier J, Lowe J. Solution structure and domain architecture of the divisome protein FtsN. Mol Microbiol. 2004; 52:651–660. [PubMed: 15101973]

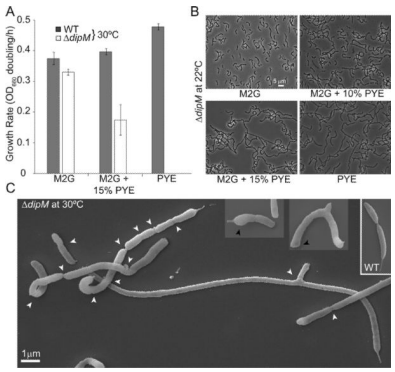

Fig. 1.

Phenotypic characterization of the Δ*dipM* mutant. (A) Growth rates (in doublings/h) of wild-type and Δ*dipM* (CJW3137) CB15N strains grown at 30°C in liquid cultures containing M2G minimal medium, M2G medium supplemented with 15% of rich PYE medium, or PYE medium. Average values and standard deviations for three experiments are shown. (B) Phase contrast images of Δ*dipM* cells grown at 22°C in different media. Δ*dipM* cells from overnight M2G cultures at 30°C were used to inoculate culture tubes containing M2G medium, PYE medium or M2G supplemented with 10 or 15% of PYE medium, which were then incubated at 22°C for an additional 24 h prior to imaging. At the time of imaging, the cultures were at an $OD_{660} \leq 0.5$. (C) Scanning EM images of Δ*dipM* mutant cells grown at 30°C in liquid M2G medium. White and black arrows indicate constriction sites and bulged poles, respectively. For comparison, the inset shows scanning EM images of a wild-type predivisional cell grown under the same conditions.

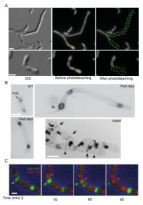

Fig. 2.

Characterization of the cell filamentation phenotype associated with the Δ*dipM* mutation. (A) FLIP experiment of diffusible cytosolic GFP expressed in Δ*dipM* cell filament (strain CJW3449) to assess the extent of cell compartmentalization. Yellow dotted circles indicate the regions targeted for photobleaching. The green dotted lines show the extension of the cytoplasmic space as determined by the extent of bleaching.(B) Transmission electron micrographs of isolated sacculi from wild-type (CB15N), Δ*dipM* (CJW3137), FtsZ-depleted (YB1585) and FtsA-depleted (CJW3187) cells. Depletion was achieved by growing cells in the absence of xylose (inducer) for 5 h (FtsZ) or 8 h (FtsA). In the wild-type panel, the arrow points to a PHB (polyhydroxybutyrate) granule trapped in the sacculus. In the Δ*dipM* panel, the arrowheads and arrows indicate PG-rings and SP-rings, respectively. (C) Selected frames from a time-lapse microscopy sequence of a Δ*dipM* cell filament (CJW3448) expressing FtsZ-YFP (green) and MipZ-CFP (red). *ftsZ-yfp* expression was induced by the addition of 0.3% xylose for 3 h prior to the start of the time-lapse experiment. In all panels, the scale bars correspond to 1 μm.

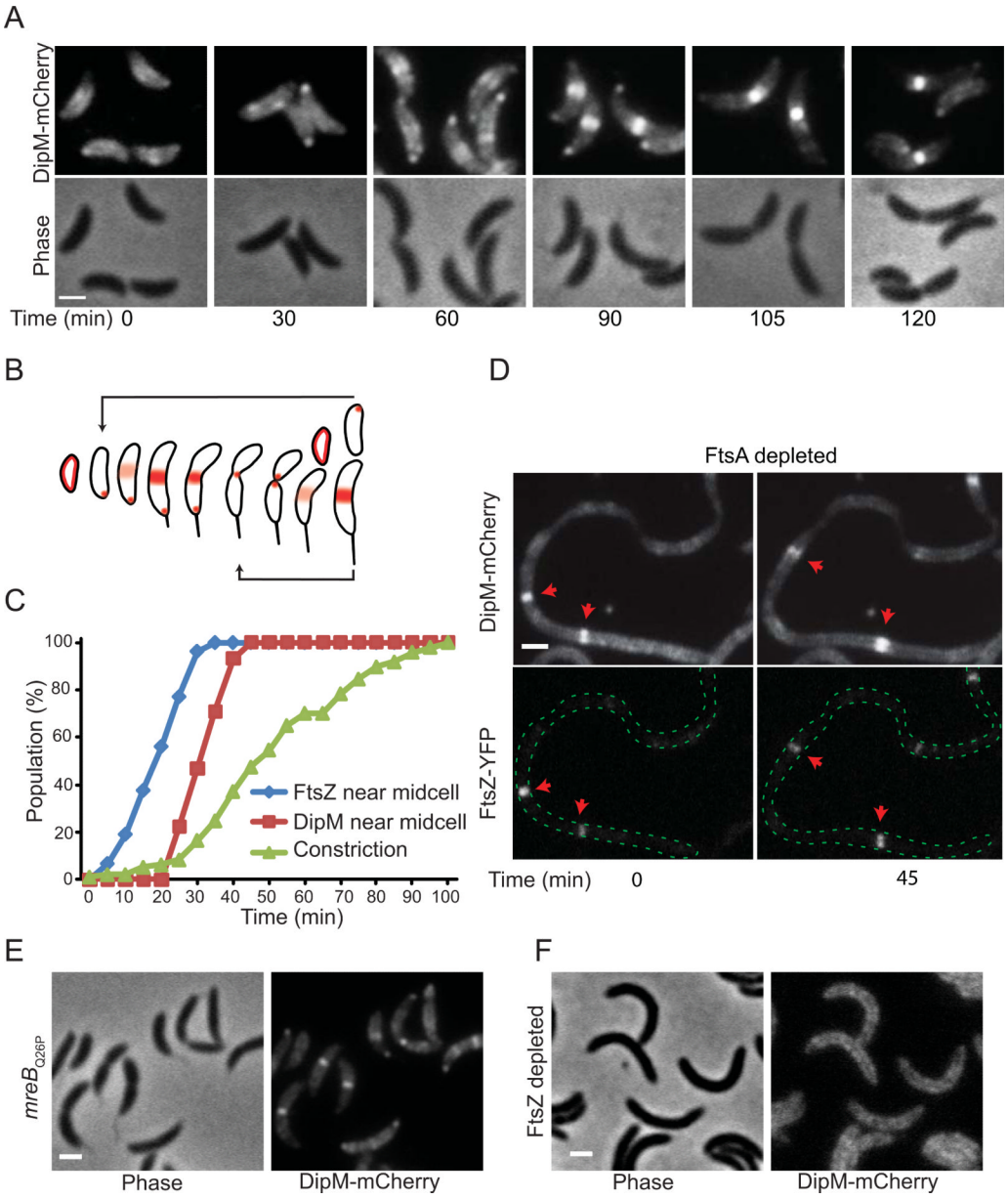

Fig. 3.

Localization of DipM during the cell cycle and its dependence on other division proteins. (A) Time-course microscopy of synchronized cells (CJW3124) expressing *dipM-mCherry* as the only copy of *dipM* from the native chromosomal promoter and progressing through the cell cycle following synchronyzation. Time 0 corresponds to purified swarmer cells resuspended in M2G medium at 30°C. (B) Schematic of the localization pattern of DipM determined from time-lapse experiments using synchronized cell cycle populations as in (A) and Movie S6. (C) The percentage of cells with DipM-mCherry and FtsZ-YFP localization near midcell and with discernible cell constriction were plotted over time. The data were obtained from two independent time-course experiments (137 and 196 cells) starting with synchronized swarmer cells (CJW3436) that were followed through a cell cycle while growing on a M2G-agarose pad. (D) Localization of DipM-mCherry in FtsA-depleted cells. Cultures of CJW3447 cells carrying *ftsA* under xylose-inducible expression were grown to an OD_{660} of 0.1 in M2G medium supplemented with 0.3% xylose (inducer), after which the

cells were washed and resuspended in M2G medium lacking xylose. After about 4 h of FtsA depletion and cell filamentation, fluorescent images of FtsZ-YFP and DipM-mCherry were acquired. *ftsZ-yfp* expression was induced with vanillic acid (250 μM) for 3 h prior to imaging. (E) DipM-mCherry localization in the $mreB_{Q26P}$ mutant (strain CJW3437). (F) DipM-mCherry localization in FtsZ-depleted cells. Cultures of CJW3438 cells carrying *ftsZ* under xylose-inducible expression and *dipM-mCherry* under the native promoter were grown to an OD_{660} of 0.1 in M2G medium supplemented with 0.3% xylose (inducer), after which the cells were washed, resuspended in M2G medium lacking xylose and spotted in an agarose pad of the same media. Depletion was followed by microscopic observation during which fluorescent images of DipM-mCherry were acquired. The image corresponds to about 4 h of FtsZ depletion and cell filamentation. The white scale bars correspond to 1 μm.

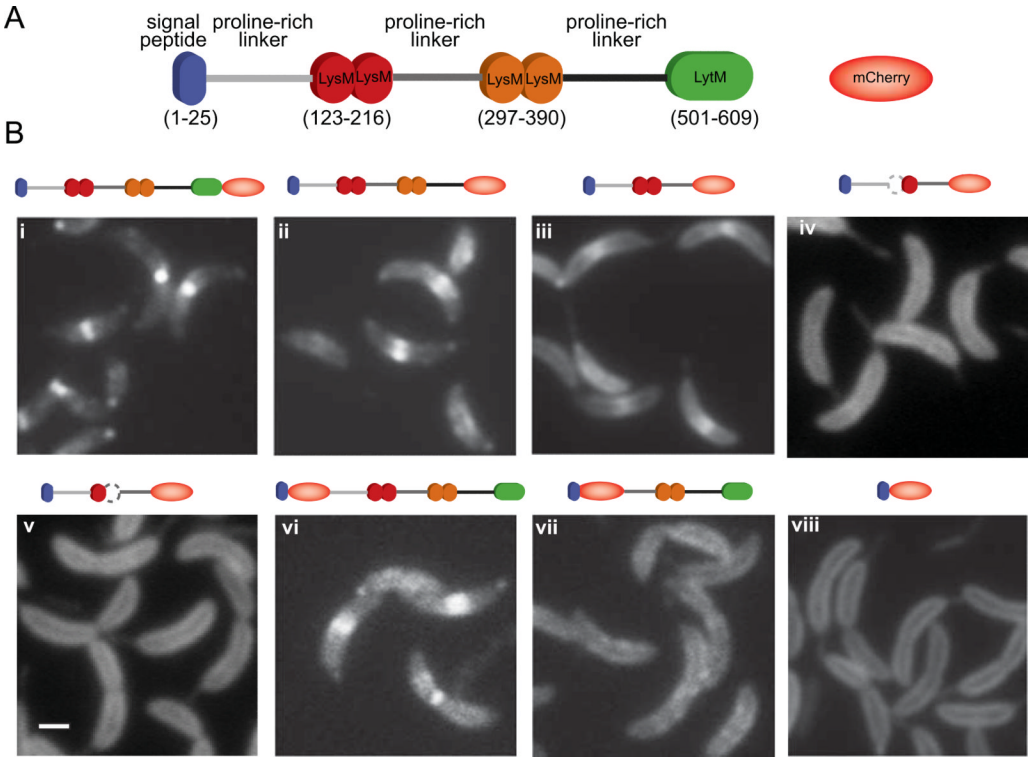

Fig. 4.

Determination of the DipM region involved in protein localization. (A) Schematic of the DipM domain organization and representation of mCherry. (B) Fluorescent micrographs of mCherry fused to different fragments of DipM: (i) DipM-mCherry (CJW3124); (ii) $DipM_{\Delta 501\text{-}609}$-mCherry (CJW3439); (iii) $DipM_{\Delta 297\text{-}609}$-mCherry (CJW3121); (iv) $DipM_{1\text{–}296\Delta 121\text{–}167}$-mCherry (CJW3526); (v) $DipM_{1\text{–}296\Delta 175\text{–}223}$-mCherry (CJW3528); (vi) mCherry-$DipM_{\Delta 1\text{-}30}$ (CJW3116); (vii) mCherry-$DipM_{\Delta 1\text{-}236}$ (CJW3117); (viii) $DipM_{\Delta 54\text{-}609}$-mCherry (CJW2959). All inducible mCherry fusions were expressed from the chromosome by adding vanillic acid to a final concentration of 250 μM about 5 to 6 h prior to microscopy. In the case of the N-terminal mCherry fusions, the signal peptide is encoded by the vector. Note that wild-type DipM is also produced in these backgrounds. The white bar corresponds to 1 μm.

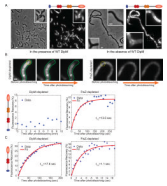

Fig. 5.

Localization and mobility of the DipM LysM tandems in FtsZ- and DipM-depleted cells. (A) Localization of the localization-proficient, inactive $DipM_{\Delta 501\text{-}609}$-mCherry fusion in CJW3446 cells inducing the synthesis of wild-type DipM (growth in the presence of 250 μM of the vanillic acid inducer), or repressing the synthesis of wild-type DipM (growing without vanillic acid inducer). (B) FRAP experiments of $DipM_{\Delta 501\text{-}609}$-mCherry (carrying two LysM tandems) in DipM- or FtsZ-depleted CJW3446 cells (n=21 and 20, respectively). Depletion of DipM or FtsZ was achieved by removing vanillic acid or xylose from the cultures for about 24 and 5 h, respectively. Regions within cell filaments were photobleached with a 1s laser pulse series. *Top*, examples of fluorescent images of $DipM_{\Delta 501\text{-}609}$-mCherry in DipM- and FtsZ-depleted cells before and after photobleaching. The photobleached regions are indicated by yellow dotted circles. The scale bar corresponds to 1 μm. *Bottom*, the percentage of fluorescence recovery was plotted as a function of time following photobleaching. The average values and the best fit (see Material and methods) are shown in blue and red, respectively. (C) FRAP experiments of $DipM_{\Delta 297\text{-}609}$-mCherry (carrying a single LysM tandem) in DipM- or FtsZ-depleted cells (CJW3445 and CJW3530, respectively). Regions of cell filaments were photobleached with a 300ms laser pulse series. Quantification was performed as in panel (B).

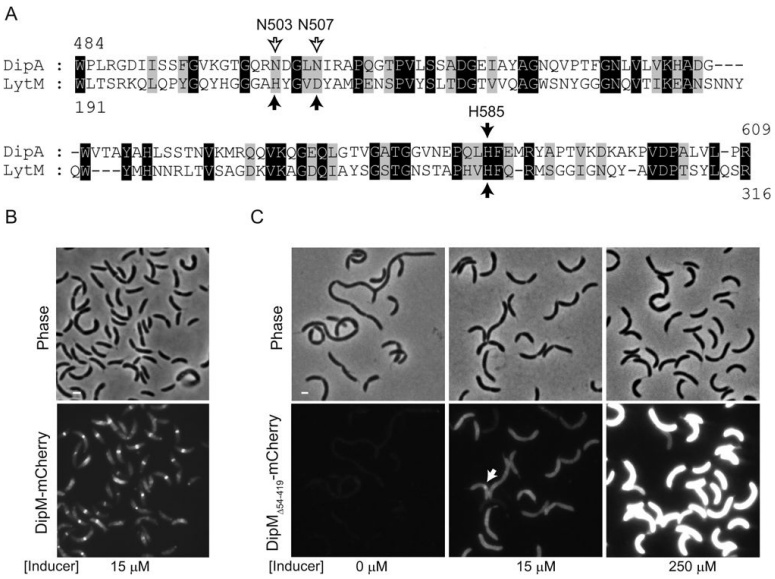

Fig. 6.

The non-canonical LytM domain of DipM can support function. (A) Alignment between *S. aureus* LytM catalytic domain and the non-canonical LytM domain of *C. crescentus* DipM. Black arrows indicate the conserved residues that are directly involved in metal coordination in the crystal structure of *S. aureus* LytM. The empty arrows indicate the non-conserved residues in DipM at positions of metal coordination. (B) Images of Δ*dipM* cells expressing wild-type *dipM* fused to *mCherry* (strain CJW3440). The cells were grown in the presence of 15 μM vanillic acid (inducer) for 5 h in M2G medium at 30°C to induce the synthesis of the mCherry fusions. Under these conditions, the level of expression of wild-type *dipM* allele was sufficient to fully suppress the cell filamentation phenotype caused by the Δ*dipM* mutation. (C) Images of Δ*dipM* cells carrying the non-canonical LytM domain of DipM (and no LysM domains) fused to mCherry (DipM$_{\Delta 54–419}$-mCherry; strain CJW3444). Different levels in DipM$_{\Delta 54–419}$-mCherry proteins were obtained by growing the cells in the presence of different concentrations of the vanillic acid inducer. The arrow indicates an example of the infrequent accumulation of DipM$_{\Delta 54-419}$-mCherry signal at constriction sites.

Table 1

List of strains used in this study.

Strain	Genotype	Source
C. crescentus		
CB15N	synchronizable derivative of *C. crescentus* CB15 (also known as NA1000)	(Evinger and Agabian, 1977)
CJW1715	CB15N *mreB*$_{Q26P}$	(Aaron *et al.*, 2007)
CJW2959	CB15N *vanA*::pVsigpepCHYN-4	(Takacs *et al.*, 2010)
CJW3116	CB15N *dipM*::pVspCHYdipM$_{\Delta 1\text{-}30}$	This study
CJW3117	CB15N *dipM*::pVspCHYdipM$_{\Delta 1\text{-}236}$	This study
CJW3121	CB15N *vanA*::pVdipM$_{\Delta 297\text{-}609}$CHY	This study
CJW3122	CB15N *dipM*::pVdipM$_{\Delta 501\text{-}609}$CHY	This study
CJW3124	CB15N *dipM*::pCHYCdipM	This study
CJW3137	CB15N Δ*dipM*::Ω–Spc	This study
CJW3187	CB15N *ftsA*::pXMCS2ftsA	This study
CJW3430	CB15N Δ*dipM*::Ω–Spc *vanA*::pMT383	This study
CJW3436	CB15N *dipM*::pCHYCdipM *vanA*::pMT383	This study
CJW3437	CB15N *mreB*$_{Q26P}$ *dipM*::pdipMCHY	This study
CJW3438	CB15N *ftsZ*::pBJM *dipM*::pCdipMCHY	This study
CJW3439	CB15N *vanA*::pVdipM$_{\Delta 501\text{-}609}$CHY	This study
CJW3440	CB15N Δ*dipM*::ΩSpc/pRVdipMCHY	This study
CJW3444	CB15N Δ*dipM*::ΩSpc /pRVCHYCdipM$_{\Delta 54\text{-}419}$	This study
CJW3445	CB15N *dipM*::pVdipM$_{\Delta 297\text{-}609}$CHY	This study
CJW3446	CB15N *dipM*::pVdipM$_{\Delta 501\text{-}609}$CHY *ftsZ*::pBJM	This study
CJW3447	CB15N *ftsA*::pXMCS2ftsA *vanA*::pMT383 *dipM*::pdipMCHY	This study
CJW3448	CB15N Δ*dipM*::Ω–Spc *vanA*::pMT383 *mipZ-cfp*	This study
CJW3449	CB15N Δ*dipM*::Ω–Spc *xylX*::pXGFPMCS-2	This study
CJW3455	CB15N *vanA*::pMT383 *mipZ-cfp*	W. Schofield
CJW3530	CB15N *vanA*:: pVdipM$_{\Delta 297\text{-}609}$CHY *ftsZ*:: pBJM	This study
CJW3526	CB15N *vanA*::pVLysM1A	This study
CJW3528	CB15N *vanA*::pVLysM1B	This study
CJW3530	CB15N ftsZ:pBJM pVdipM$_{\Delta 297\text{-}609}$CHY	This study
CJW3550	*vanA*::pVsigpepMCHYN-4 *ftsZ*::pBJM	This study
CJW3551	Δ*dipM*::Ω–Spc *vanA*::pVsigpepMCHYN-4	This study
CJW3591	CB15 *dipM*::pdipMCHY *divE309* (*fts*Ats) Rif^{r}	This study
MT196	CB15N *vanA*::pMT383	(Thanbichler and Shapiro, 2006)
PC8848	CB15 *divE309* (*fts*Ats) Rif^{r}	(Ohta *et al*, 1997)
YB1585	CB15N *ftsZ*::pBJM	(Wang *et al.*, 2001)
E. coli		
DH5a	Cloning strain	Invitrogen
TOP10	Cloning strain	Invitrogen

Table 2

List of plasmids used in this study.

Plasmid	Characteristic	Source
pCHYC-4	pMB1 replicon with *oriT* and *mCherry*	(Thanbichler *et al.*, 2007)
pCR2.1-TOPO	Cloning vector	Invitrogen
pdipMCHY	pCHYC-4 carrying $dipM_{421\text{-}609}$	This study
pNPTS138	pLitmus38 derivative carrying *oriT* and *sacB*	MRK Alley
pNPTSΔdipM::Ω	pNPTS138 carrying Δ*dipM*::Ω-Spc	This study
pRVCHYC1	Vector with *oriT*, *oriV*, *vanAp* and *mCherry*	(Thanbichler *et al.*, 2007)
pRVdipMCHY	pRVCHYC-1 carrying *dipM*	This study
pRVdipM$_{\Delta 54\text{-}419}$CHY	pRVCHYC-1 carrying $dipM_{\Delta 54\text{-}419}$	This study
pTOPOdipM	pCR2.1-TOPO carrying *dipM*	This study
pVCHYC-4	pMB1 replicon with *oriT*, *vanAp* and *mCherry*	(Thanbichler *et al.*, 2007)
pVCHYN-4	pMB1 replicon with *oriT*, *vanAp* and *mCherry*	(Thanbichler *et al.*, 2007)
pVdipM$_{\Delta 297\text{-}609}$CHY	pVCHYC-4 carrying $dipM_{\Delta 297\text{-}609}$	This study
pVdipM$_{\Delta 501\text{-}609}$CHY	pVCHYC-4 carrying $dipM_{\Delta 501\text{-}609}$	This study
pVspCHYdipM$_{\Delta 1\text{-}30}$	pVsigpepCHYN-4 carrying $dipM_{\Delta 1\text{-}30}$	This study
pVspCHYdipM$_{\Delta 1\text{-}236}$	pVsigpepCHYN-4 carrying $dipM_{\Delta 1\text{-}236}$	This study
pVsigpepCHYN-4	pVCHYN-4 carrying $dipM_{\Delta 54\text{-}609}$	(Takacs *et al.*, 2010)
pVLysM1ACHY	pVCHYC-4 carrying $dipM_{1\text{–}296\Delta 121\text{–}167}$	This study
pVLysM1BCHY	pVCHYC-4 carrying $dipM_{1\text{–}296\Delta 175\text{–}223}$	This study
pXMCS-2	pMB1 replicon with *oriT* and *xylXp* promoter	(Thanbichler *et al.*, 2007)
pXMCS2*ftsA*	pXMCS-2 with *ftsA* under *xylXp* control	This study